Cloud masking in remotely sensed hyperspectral images using linear and nonlinear spectral mixture analysis

J. Amorós-López[1], L. Gómez-Chova[1], A. Plaza[2], J. Plaza[2], J. Calpe[1], L. Alonso[3], J. Moreno[3]
(1) GPDS, Dept. of Electronic Eng., University of Valencia (Spain)
(2) Dept. of Computer Science, University of Extremadura (Spain)
(3) LEO, Dept. of Thermodynamics and Earth Science, University of Valencia (Spain)
julia.amoros@uv.es

ABSTRACT - *In this paper, we analyze the effectiveness of spectral mixture techniques in the generation of a cloud abundance mask. Two different mixture models are considered: linear and nonlinear. The linear model first identifies pure spectral constituents (endmembers) and then expresses mixed pixels as linear combination of endmembers. It is clear that there are naturally occurring situations where nonlinear mixture models can better describe the resultant mixed spectra for certain endmember distributions. In order to address this issue, we carry out comparisons among different implementations of the linear model (e.g., using a variety of endmember extraction algorithms and constraints in the linear inversion process) and a neural network-based nonlinear model, which utilizes a multi-layer perceptron (MLP) architecture with back-propagation learning.*

Experiments are conducted on a set of CHRIS/Proba Mode 1 acquisitions with 62 spectral bands in the visible and near-infrared spectral range and spatial resolution of 34 meters. Additionally, the method is validated with a database made up of simulated images with artificially generated clouds (mixed with other materials in both linear and nonlinear fashion).

1 INTRODUCTION

The presence of clouds in satellite spectral images prevents adequate characterization of land cover, and constitutes a very important source of errors which strongly affects estimation and retrieval of bio-physical parameters (Simpson, 1999). As a result, accurate cloud masking represents both a challenge and a pre-processing requirement for the majority of techniques dealing with information extraction from remotely sensed data.

Standard cloud masking algorithms in the literature generally provide a binary mask, i.e., they consider each image pixel location as a pure entity with an associated discrete label that indicates whether the pixel is covered by a cloud or not (Di Vittorio, 2002). However, in hyperspectral analysis this approach is not appropriate. This is because, in multispectral imaging, the fine spectral resolution available can be used to overcome the so-called "mixture problem" by estimating the fractional abundance of materials at a sub-pixel level (this is particularly important in remotely sensed satellite data sets with relatively coarse spatial resolution) (Adams, 1985). By resorting to spectral mixture analysis-based techniques, it is possible to model additional application scenarios, e.g., when thin clouds, such as cirrus, partially cover a given pixel (with different degrees of transparency), or when thicker clouds do not entirely cover the pixel. In those cases, sub-pixel techniques such as those based on spectral unmixing can provide a more accurate characterization of detected clouds in terms of different parameters (e.g., cloud type, height, sub-pixel coverage, etc.). These characteristics can provide a better description of the detected clouds in order to include this information in the climate models (Tian, 1999). It is also noticeable that, in linear mixing models, the endmembers are assumed to be sitting side-by-side within the field of view of the imager, and the collection procedure does not consider secondary reflections and/or multiple scattering effects, which may be particularly relevant in the case of clouds.

In this paper, we mainly analyze spectral mixing techniques to generate synthetic images with cirrus clouds using both linear and nonlinear mixing. This simulated dataset allows evaluating the proposed methodology, and it makes up for the lack of ground truth data to validate the real image results.

The paper is outlined as follows. Section 2 explains the employed real and simulated datasets. Section 3 describes the methodology. The results are presented in Section 4, and the conclusions are given in Section 5. Finally, we conclude with acknowledgements and references.

2 DATASET

2.1 Real Dataset

One image of the CHRIS (Compact High Resolution

Figure 1. *Selected image with cumulus and thin cirrus clouds. Hinton (Canada).*

Imaging Spectrometer) instrument on board of PROBA satellite has been considered in this study. CHRIS Mode 1 provides 62 spectral bands in the spectral range from 400 to 1050nm with a 34m spatial resolution (Barnsley, 2004, and PROBA/CHRIS web). The selected image is located in Hinton (Lat/Lon: 53.14,-117.145), Canada, and was acquired on 2006-07-11. The image presents two types of clouds, small cumulus and thin cirrus clouds (Fig.1).

The satellite image has been preprocessed in order to reduce sensor noise and to obtain illumination independent data (TOA reflectance) (Chova, 2005).

2.2 Simulated Dataset

Synthetic images are generated using spectra extracted from the real CHRIS/PROBA image using the Iterative Error Analysis (IEA) endmember extraction algorithm (Neville, 1999). We assume Gaussian distributions to generate the mixed spectra by using the full covariance matrix of each class. Two different mixing models are considered:

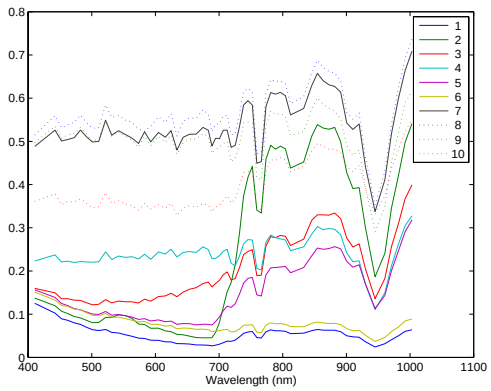

Figure 2. *Extracted endmembers by the Iterative Error Analysis algorithm.*

a) Linear mixing: In this model, the reflectance spectrum ρ is considered as a standard linear combination of the "pure" spectra or *endmembers* (s_i) of the materials present in the pixel area, weighted by their fractional abundance (α_i). This linear mixing model (Adams, 1985 and Settle, 1993) is the most frequently used model for representing the mixed pixels from different endmembers and is expressed as:

$$\rho = \sum_{i=1}^{N} \alpha_i \cdot s_i + \varepsilon = \mathbf{S} \cdot \alpha + \varepsilon \qquad (1)$$

where N is number of endmembers and ε is the allowed error noise.

The linear synthetic image is generated using the endmembers extracted by IEA algorithm (Fig.2) and the spatial distribution of the abundance generated for each *endmember*.

b) Non linear mixing for clouds: There are many situations where nonlinear processes are present in the scene (*endmember* materials are mixed on spatial scales smaller that pixel size, multiple scattering, atmospheric absorptions, etc.). In this paper, we propose a nonlinear mixing model where the pixel surface reflectance is mixed with a cloud spectrum at different degrees of transparency (cloud transmittance, $1-\alpha \cdot \rho_c$). In this model, we take into account the multiple scattering effects as is depicted in Fig. 3, which can be expressed as:

$$\rho_T = \alpha \cdot \rho_c + (1-\alpha \cdot \rho_c)^2 \rho_g \left(1 / 1 - \rho_g \alpha \cdot \rho_c \right) \qquad (2)$$

where ρ_T is the apparent reflectance of the mixed pixel, ρ_c is cloud reflectance, and ρ_g is ground reflectance. Note that, in this model, we have considered clear atmosphere and no cloud absorption.

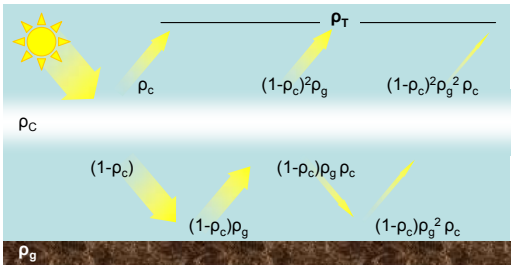

Figure 3. *Nonlinear mixing diagram.*

3 METHODOLOGY

3.1 Spectral Unmixing

Spectral unmixing allows decomposing the measured mixed spectrum into a collection of constituent spectra or *endmembers*, and a set of corresponding abundances that indicate the proportion of each *endmember* in the pixel. Spectral unmixing can be considered as two separate problems: first, the determination of the endmembers, and then the estimation of the abundances.

3.1.1 *Endmember* extraction algorithms

In the literature, there are different approaches to determine the spectra of the different pure constituents in the image (Keshava, 2002 and Plaza, 2006). We have selected three different methods to extract the pure pixels from the image.

a) ATGP: Automated Target Generation Process (Ren, 2003, and Chang, 2003).

b) IEA: Iterative Error Analysis (Neville, 1999).

c) VCA: Vertex Component Analysis (Nascimento, 2005).

3.1.2 Linear Unmixing Model

The fraction of each pixel in the linear spectral unmixing is obtained by solving the inverse equation of the linear mixel model that is expressed as:

$$\alpha + \varepsilon = S^{-1} \cdot \rho_T \qquad (3)$$

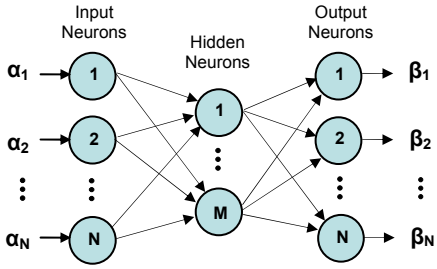

Figure 4. *Multilayer Perceptron Architecture.*

Additionally, we can impose that the linear unmixing is subjected to two constrains with full physical meaning.

a) Fully Constrained Least Squares Unmixing (FCLSU): In FCLSU (Heinz, 2001), two intuitive restrictions are imposed to equation 3.

- Abundance sum-to-one constraint: the abundance fractions of all the targets must sum one.

$$\sum_{i=1}^{N} \alpha_i = 1 \quad or \quad \mathbf{1}^T \alpha = 1 \qquad (4)$$

- Abundance non-negativity constraint: abundance fractions of all targets must be nonnegative (since they represent the abundance or contribution of reflectance spectral signatures).

$$0 \le \alpha \le 1 \qquad (5)$$

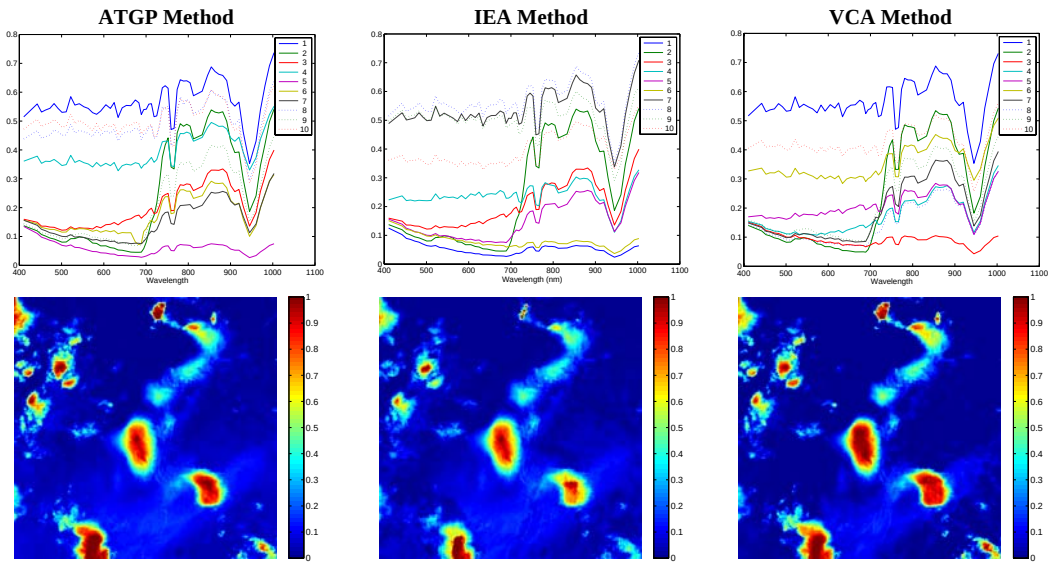

Figure 5. *Pure pixels selected by the three endmember methods (top) and Cloud Abundance Map obtained from FCLSU unmixing using the different endmember sets (bottom).*

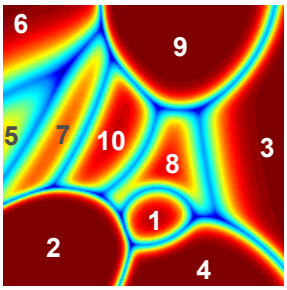

Figure 6. *Simulated regions (1-Shadows, 2-Veg, 3-Soil, 4-Soil and thin cloud, 5- Veg, 6- Shadows, 7-High Cloud, 8- High Cloud, 9-High Cloud, and 10- Cloud).*

b) Non-Negativity Constrained Least Squares Unmixing (NNCLSU): In this approach, only the non-negativity constrain is considered to account for the possibility of an incomplete set of endmembers.

3.1.3 Nonlinear Unmixing Model

In the case of nonlinear unmixing, a neural network (NN) is used as the nonlinear correction to the linear model. A multi-layer perceptron (MLP) NN is used as a subsequent processing step after the FCLSU unmixing model (Plaza, 2005).

The abundances provided by the FCLSU (α) are used as the inputs of the MLP network (Fig 4), and the outputs are the corrected abundances of the simulated images (β).

In this paper, two MLP networks have been trained. One MLP-NN is trained using data from the linearly mixed image in order to compare it with the FCLSU, which should provide good abundance fractions without the NN correction step. Another MLP network is trained for the nonlinear image to improve the results under nonlinear effects.

3.2 Cloud Map

Unmixing methods provide an output image with N bands showing the proportion of each *endmember* in each pixel, being N the number of endmembers.

In order to obtain a cloud map from the abundances, the endmembers corresponding to cloud covers have to be identified. The identification of the cloud endmembers is performed by the user taking into account the spectral signature, their abundance map, and their location. Finally, the cloud abundance map is obtained as the sum of all the abundance maps corresponding to cloud endmembers.

4 RESULTS

4.1 Real Data

We have applied the three *endmember* extraction algorithms to the Hinton image, and we have obtained the pure spectra that are shown at the top of Fig. 5. The extraction algorithms methods are analyzed in different images for a thorough evaluation, and results show that a good selection of the endmembers is the

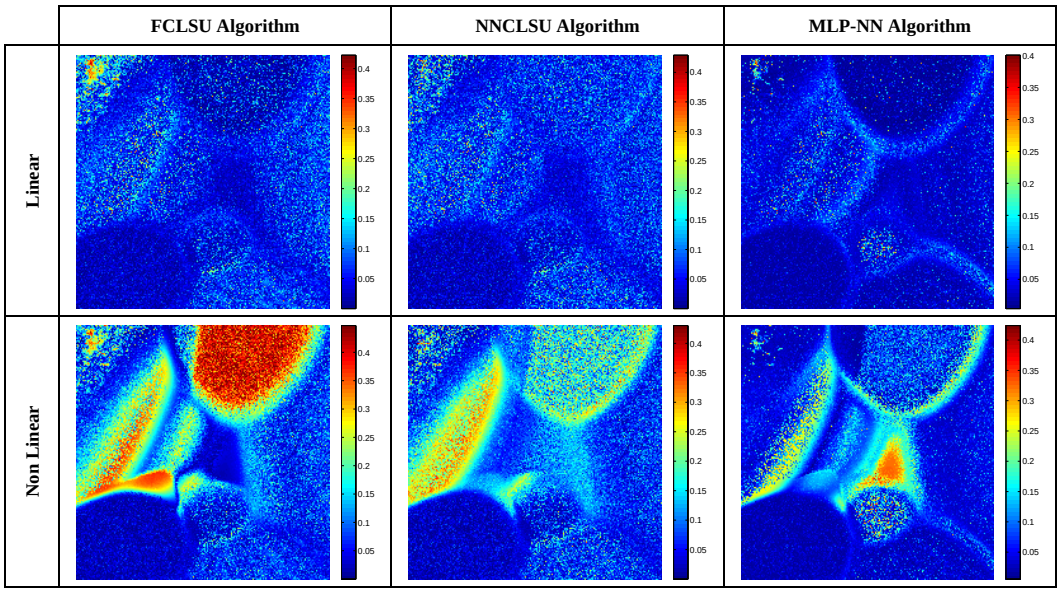

Figure 7. *RMSE between the estimated abundance and the real values for the simulated linear (top) and non linear (bottom) images. Note that the colour scales are not the same.*

Simulated Image		RMSE	Cloud-RMSE	r	Cloud-r
Linear	FCLSU	0.0751	**0.0095**	0.960	0.997
	NNCLSU	0.0759	0.0127	0.959	0.994
	MLP-NN	**0.0522**	0.0100	0.980	0.996
Non Linear	FCLSU	0.1824	0.0184	0.727	0.986
	NNCLSU	0.1320	0.0209	0.863	0.991
	MLP-NN	**0.1021**	**0.0128**	0.920	0.994

Table 1. *RMSE and correlation coefficient (r) between the real and unmixed abundances, for all the endmembers and only for cloud endmembers.*

most critical point in the unmixing process. In the case of clouds, more than one *endmember* of clouds are obtained for the same image.

Then, the proportional abundances of each *endmember* are calculated by the FCLSU unmixing method, and finally, we sum the different cloud abundances in order to obtain the final cloud abundance map (Fig. 5 bottom). For the case of this image, the IEA method seems to provide the best endmembers for cloud mapping, as it detects better the cirrus clouds.

Results using the NNCLSU method are quite similar to FCLSU.

4.2 Simulated Data

The three unmixing algorithms introduced in section 3 (FCLSU, NNCLSU and Neural Network) are applied to obtain the abundance map for each *endmember*. The unmixing accuracy is assessed in terms of the root mean square error (RMSE) and correlation coefficient (r) between the original and obtained abundances.

Fig. 6 shows the map of the simulated regions and Fig. 7 the error images. We can observe that in both linear and nonlinear cases, the MLP reduces the error in the different classes, but not so much in the border areas, where non-linear effects are more important.

Table 1 shows results obtained with the three presented unmixing methods for both the linear and non linear simulated images. Assessment of the unmixing results is performed by computing the RMSE and correlation coefficient between the real and the unmixed abundances. In addition, we compute the errors between the real and estimated cloud abundances (Cloud-RMSE), where the cloud-abundance is defined as the sum of the abundances of all the cloud-endmembers. Even though the MLP-NN provides better results in the simulated image, it is not the case when we analyze only the errors in the cloud abundances. From Table 1, three issues should be noticed:

- Considering separately the abundances of all the endmembers (RMSE), the MLP-NN provides better results than the LSU methods since the training set helps to accurately estimate abundances of similar endmembers, and also corrects the non-linearity of the spectral mix.
- Considering only the abundance of the cloud endmembers (Cloud-RMSE), the FCLSU produces lower errors in the linear mixed image since the confusion between similar spectral endmembers does not affect to the combined cloud abundance. As in the previous case, the MLP-NN provides better results for the non-linear mixing.
- The RMSE obtained for NNCLSU is not comparable with the other methods because its abundances are not required to sum one, while for the reference simulated images they do.

5 CONCLUSIONS

In this work, we have analyzed two linear and one nonlinear spectral unmixing techniques with CHRIS/PROBA images presenting cirrus clouds, and with synthetic images generated with both a linear and nonlinear mixing approaches.

The main conclusions extracted from both experiments are the following.

Results showed that, for all the unmixing methodologies, the final cloud abundance map is very sensitive to the *endmember* identification.

When unmixing the linearly mixed synthetic image:

- FCLSU and NNCSLU provide similar results.
- MLP Neural Network reveals useful to reduce the impact of the variability within class due to the additional information provided by the supervised training.

When unmixing the non-linearly mixed image:

- FCLSU and NNCSLU tend to favour the *endmember* with a greater similarity to the given spectrum, in detriment of other endmembers, thus reducing the accuracy in abundance.
- MLP Neural Network reduces slightly the errors but the results are not as robust as expected, especially in those regions where non-linear mixing is more important.

The approach of using the LSU as input to the NN for non-linear unmixing might not be adequate since it eliminates the second order mixture information. Thus, better results could be obtained using

directly a set of spectral bands (or extracted features) as input patterns for the MLP Neural Network.

ACKNOLEDGEMENTS

This paper has been partially supported by the Ministerio de Educación y Ciencia of Spain under the project DATASAT (ESP2005-07724-C05-03). The authors would like to acknowledge Prof. J.D. Martín and L. Guanter from University of Valencia for their valuable help, and also ESA and Sira for the availability of CHRIS/PROBA images.

REFERENCES

Adams, J.B., Smith, M.O., and Johnson, P.E., 1985, Spectral mixture modeling: A new analysis of rock and soil types at the Viking Lander 1 site. *Journal of Geophysical Research*, 91(B8), pp. 8090-8112.

Barsnley, M., Settle, J., Cutter, M., Lobb, D., and Teston, F., 2004, The PROBA/CHRIS mission: a low-cost smallsat for hyperspectral, multi-angle, observations of the Earth surface and atmosphere. *IEEE Trans. On Geoscience and Remote Sensing*, 42(7), pp. 1512-1520.

Chang, C.-I., 2003, Hyperspectral imaging: spectral detection and classification. Kluwer Academic Publishers.

Di Vittorio, A.V., and Emery, W.J., 2002, An automated, dynamic threshold cloud-masking algorithm for daytime AVHRR images over land. *IEEE Trans. On Geoscience and Remote Sensing*, 40(8).

Gomez-Chova, L., Amorós, J., Camps-Valls, G., Martín, J., Calpe, J., Alonso, L., Guanter, L., Fortea, J., and Moreno, J., 2005, Cloud masking scheme based on spectral, morphological, and physical features. In *3rd CHRIS/Proba Workshop*, ESA-SP-593, ed., ESRIN, Frascati, Italy.

Heinz, D., and Chang, C.-I., 2001, Fully constrained least squares linear mixture analysis for material quantification in hyperspectral imagery. *IEEE Trans. On Geoscience and Remote Sensing*, 39, pp. 529-545.

Keshava, N., and Mustard, J.F., 2002, Spectral Unmixing. *IEEE Signal Processing Magazine*, 19(1), pp. 44-57.

Nascimento, J.M.P., and Dias, J.M.B., 2005, Vertex Component Analysis: A fast algorithm to unmix hyperspectral data. *IEEE Trans. On Geoscience and Remote Sensing*, 43(4), pp. 898-910.

Neville, R.A., Staenz, K., Szeredi, T., Lefebvre, J., and Hauff, P., 1999, Automatic endmember extraction from hyperspectral data for mineral exploration. *4th International Airborne Remote Sensing Conf. and Exhibition/21st Canadian Symposium on Remote Sensing*, Ottawa, Ontario, Canada, pp. 21-24.

Plaza, A., and Chang, C.I., 2006, Impact of initialization on design of endmember extraction algorithms. *IEEE Transactions on Geoscience and Remote Sensing*, 44(11), to appear in Nov. 2006.

Plaza, J., Chang, C.-I., Plaza, A., Perez, R., and Martinez, P., 2005, On the generation of training samples for neural network-based mixed pixel classification. *Conference on Algorithms and Technologies for Multispectral, Hyperspectral and Ultraspectral Imagery XI*, SPIE Symposium on Defense and Security, SPIE Vol. 5806, Orlando, Florida, USA.

PROBA/CHRIS mail web page: http://www.CHRIS-PROBA.org.uk/

Ren, H., and Chang, C.-I., 2003, Automatic spectral target recognition in hyperspectral imagery. *IEEE Transactions On Aerospace and Electronic Systems*, 39(4), pp. 1232-1249.

Settle, J.J., and Drake, N.A., 1993, Linear mixing and the estimation of ground cover proportions. *International Journal of Remote Sensing*, 14, pp. 1159-1177.

Simpson, J., 1999, Improved cloud detection and cross-calibration of ATSR, MODIS and MERIS data. In *ATSR International Workshop on the Applications of the ERS along track scanning radiometer*, ESA-SP-479, ed., ESRIN, Frascati, Italy.